Flow adjustment and interior flow associated with a rectangular porous obstruction

J. Fluid Mech. (2011), *vol.* 680, *pp.* 636–659.
doi:10.1017/jfm.2011.199

Flow adjustment and interior flow associated with a rectangular porous obstruction

JEFFREY T. ROMINGER AND HEIDI M. NEPF

Department of Civil and Environmental Engineering, Massachusetts Institute of Technology, Cambridge, MA 02139, USA

(Received 30 July 2010; revised 28 February 2011; accepted 1 May 2011; first published online 13 June 2011)

The flow at the leading edge and in the interior of a rectangular porous obstruction is described through experiments and scaling. The porous obstruction consists of an emergent, rectangular array of cylinders in shallow flow, a configuration that mimics aquatic vegetation. The main features of the flow depend upon the non-dimensional canopy flow-blockage, which is a function of the obstruction width and porosity. For the ranges of canopy flow-blockage tested in this paper, the fluid decelerates upstream of the obstruction over a length scale proportional to the array width. For high flow-blockage, the interior adjustment length within the porous obstruction is set by the array width. For low flow-blockage, the array's frontal area per unit volume sets the interior adjustment length. Downstream of the adjustment regions, the interior velocity is governed by a balance between the lateral divergence of the turbulent stress and canopy drag, or by a balance between the pressure gradient and canopy drag, depending on the lateral penetration into the array of Kelvin–Helmholtz (KH) vortices, which is set by the non-dimensional canopy flow-blockage. For a porous obstruction with two stream-parallel edges, the KH vortex streets along the two edges are in communication across the width of the array: a phenomenon that results in cross-array vortex organization, which significantly enhances the vortex strength and creates significant lateral transport within the porous obstruction.

Key words: coastal engineering, mixing and dispersion, shallow water flows

1. Introduction

There are many examples of flow encountering fixed, porous obstructions. For generality, we will refer to all such obstructions as canopies. Man-made canopies include urban areas with close groupings of buildings and wind farms. Terrestrial and aquatic vegetation is often organized in canopies. Coastal ocean canopies include coral reefs, seagrasses and kelp forests. Agricultural fields are porous obstructions, organized in regular rows and aquaculture, such as oyster farms, are dense underwater canopies in estuarine zones.

When the height of these canopies is very small relative to the depth of flow, and it is only of interest to understand the flow structure outside of the canopy, it is sufficient to treat the canopy as surface roughness. However, when the canopy is emergent or occupies a significant fraction of the flow depth, or when the flow through the canopy has significant physical and/or biological implications, it becomes necessary to resolve the flow within it.

Many studies have looked at the effect of porous layers on flow characteristics, such as mean velocity, turbulence level and scalar and momentum flux. Beavers &

Joseph (1967) described laminar flow adjacent to a porous layer, and several authors have extended this work to describe turbulent flow adjacent to more general arrays (Raupach, Finnigan & Brunet 1996; White & Nepf 2007). In urban settings, Bentham & Britter (2003) predicted a steady-state value for the in-canopy velocity based on the element density within the array and the exterior flow speed above the canopy. Raupach *et al.* (1996) showed how the presence of a canopy creates an unstable shear layer that generates Kelvin–Helmholtz vortices, which enhance transport between the layer and the adjacent open flow. Other studies have described the parameters that set the length scale of momentum penetration from a free stream into a canopy and the size of the shear layer (Thom 1971; White & Nepf 2007). The above studies have all focused on fully developed flow, or the development of flow at the flow-parallel interface of an infinitely long canopy. However, vegetation and man-made structures rarely exist as continuous canopies, but rather are often organized in patches of finite dimensions and, specifically, have a distinct leading edge perpendicular to the direction of mean flow. Where flow encounters the leading edge of a finite-width canopy, a portion of the flow is diverted and a portion of the flow enters and advects through the length of the canopy. The fraction of flow moving through the canopy can influence the water and air quality within the canopy as well as the ecosystem function of natural canopies.

In this paper, we consider the leading edge and the interior regions of an emergent, rectangular canopy in uniform, shallow flow. In a region close to the leading edge, the velocity responds to the step change in flow resistance from only bed friction to the addition of canopy drag. This adjustment region has previously been described by a balance between fluid inertia and the streamwise canopy drag force (Jackson & Winant 1983; Belcher, Jerram & Hunt 2003; Coceal & Belcher 2004; Ghisalberti & Nepf 2009). We show that this balance is applicable in canopies with low flow-blockage in both terrestrial and aquatic flows. The canopy flow-blockage is a dimensionless parameter that is a function of the canopy solid volume fraction and the canopy width. In this paper, we also describe the different flow behaviour for canopies with high flow-blockage, for which the simple balance of fluid inertia and drag does not apply, and we define the expected transition between canopies that exhibit low and high flow-blockage behaviour.

The mean streamwise velocity in the interior of a canopy has been well described for terrestrial canopies with low flow-blockage (Belcher *et al.* 2003; Bentham & Britter 2003; Eames, Hunt & Belcher 2004); however, it is less well understood for canopies with high flow-blockage. We present new scaling arguments for high flow-blockage canopies and provide experimental data that clearly depict different interior regimes for canopies with low and high flow-blockage. Finally, we investigate the role played by the KH vortices that form at the two flow-parallel interfaces in the transport of momentum and scalars to the canopy interior.

2. Problem description and scaling analysis

2.1. *Patch geometry*

We consider a finite rectangular canopy located in a fluid of depth h. The canopy is emergent, i.e. its height is greater than or equal to the water depth, and the canopy is uniform over the depth such that the system can be approximated as two-dimensional. The canopy length is parallel to the mean flow direction with velocities u and v in the streamwise and transverse directions, respectively. The x-axis is parallel to the mean flow and sits along the centreline of the array. The y-axis is at the leading edge

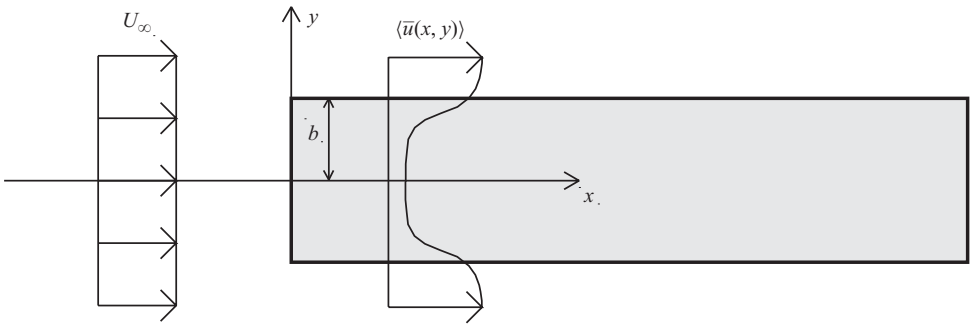

FIGURE 1. Plan view of a rectangular porous obstruction in a uni-directional current with steady and uniform velocity, U_∞, upstream.

of the canopy and is perpendicular to the mean flow direction (figure 1). The array is described by its half-width, b. The full width of the canopy perpendicular to the oncoming flow is $B = 2b$. We restrict our analysis to canopies where the overall length is much larger than the canopy width, and where the canopy width is much smaller than the flow domain.

In these experiments, the canopy half-width is geometrically similar to the height of urban, terrestrial or submerged canopies, for which the flow passes over the top of the canopy and $y = 0$ is the impermeable ground. However, there are important differences between terrestrial canopies and the shallow water configuration that we study in this paper. The upstream velocity profile for canopies in shallow water is uniform (figure 1), while for terrestrial canopies the upstream flow profile is logarithmic. Furthermore, shallowness inhibits large-scale three-dimensional turbulence, while in deeply submerged aquatic canopies or in terrestrial canopies, this large-scale turbulence can play a role in the transport of momentum and scalars. Submerged canopies have been classified as sparse or dense based on the magnitude of canopy drag relative to the bed shear stress (see table 1 in § 2.2.4). Dense canopies contribute sufficient drag to transform the velocity profile into a mixing layer form (Raupach *et al.* 1996). In the limit of very sparse submerged aquatic canopies or very sparse terrestrial canopies, the velocity profile remains logarithmic and the canopy behaves like bed roughness (Finnigan 2000; Belcher *et al.* 2003).

In this study, the model canopy elements have a diameter, d, and the mean spacing between the centres of two adjacent elements is s (figure 2). The solid volume fraction, ϕ, is the volume within the canopy occupied by solid elements, which is the complement of the canopy porosity, $\eta = 1 - \phi$. The frontal area per unit volume of the canopy is $a = nd$, where n is the number of elements per unit planar area. Within the array, the flow is both unsteady in time and spatially heterogeneous at the scale of the individual elements. A double-averaging method is used to remove the temporal and element-scale spatial heterogeneity (Gray & Lee 1977; Raupach & Shaw 1982; Nikora *et al.* 2007). The instantaneous equations are first averaged over a period of time longer than the time scale of turbulence or instabilities in the flow. The time-averaged equations are then averaged over an area of size s^2 including only area occupied by the fluid. The spatial average is denoted by angled brackets and an overbar indicates the time average. The parameter a is valid only for length scales longer than the canopy spacing, s, and therefore in a small region near the leading edge the definition of a breaks down. However, in all of the arrays tested in this

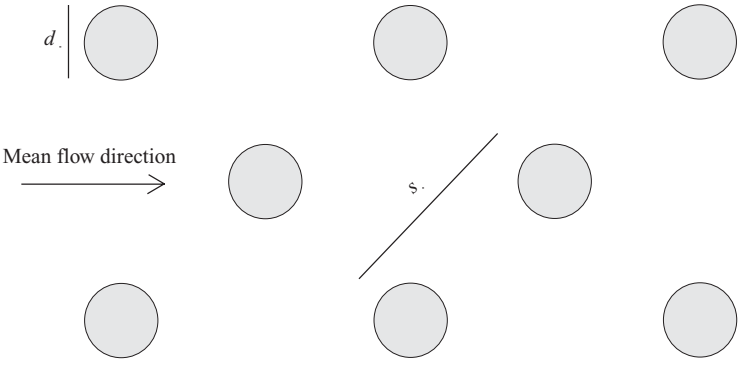

FIGURE 2. Plan view of the array elements, with diameter, d, and spacing, s.

paper, the element spacing, s, is much smaller than the length scales of the array, and the definition of a is sufficient for our analysis.

2.2. *Canopy regions and governing equations*

2.2.1. *Governing equations*

The shallow water equations for continuity, streamwise momentum and cross-stream momentum are

$$\frac{\partial h\langle\overline{u}\rangle}{\partial x} + \frac{\partial h\langle\overline{v}\rangle}{\partial y} = 0, \tag{2.1}$$

$$\frac{\partial h\langle\overline{u}\rangle\langle\overline{u}\rangle}{\partial x} + \frac{\partial h\langle\overline{v}\rangle\langle\overline{u}\rangle}{\partial y} = -\frac{1}{\rho}\frac{\partial h\langle\overline{p}\rangle}{\partial x} + \frac{1}{\rho}\left[\frac{\partial h\langle\overline{\tau_{xx}}\rangle}{\partial x} + \frac{\partial h\langle\overline{\tau_{xy}}\rangle}{\partial y}\right] - hF_x, \tag{2.2}$$

$$\frac{\partial h\langle\overline{u}\rangle\langle\overline{v}\rangle}{\partial x} + \frac{\partial h\langle\overline{v}\rangle\langle\overline{v}\rangle}{\partial y} = -\frac{1}{\rho}\frac{\partial h\langle\overline{p}\rangle}{\partial y} + \frac{1}{\rho}\left[\frac{\partial h\langle\overline{\tau_{yx}}\rangle}{\partial x} + \frac{\partial h\langle\overline{\tau_{yy}}\rangle}{\partial y}\right] - hF_y, \tag{2.3}$$

in which u and v are the fluid velocities in the x and y directions, respectively, h is the flow depth, ρ is the fluid density, p is the fluid pressure and τ is the shear stress. We define F_i as the drag force exerted on the fluid in the direction i.

Outside the canopy,

$$F_x = \frac{1}{2}\frac{C_f}{h}\langle\overline{u}\rangle\left(\langle\overline{u}\rangle^2 + \langle\overline{v}\rangle^2\right)^{1/2}, \tag{2.4}$$

$$F_y = \frac{1}{2}\frac{C_f}{h}\langle\overline{v}\rangle\left(\langle\overline{u}\rangle^2 + \langle\overline{v}\rangle^2\right)^{1/2}. \tag{2.5}$$

Inside the canopy,

$$F_x = \frac{1}{2}\frac{C_D a}{(1-\phi)}\langle\overline{u}\rangle\left(\langle\overline{u}\rangle^2 + \langle\overline{v}\rangle^2\right)^{1/2}, \tag{2.6}$$

$$F_y = \frac{1}{2}\frac{C_D a}{(1-\phi)}\langle\overline{v}\rangle\left(\langle\overline{u}\rangle^2 + \langle\overline{v}\rangle^2\right)^{1/2}, \tag{2.7}$$

where C_f is the bed friction coefficient and C_D is the drag coefficient of the array elements. Outside of the canopy, $\phi = 0$. Measurements of Δh around the canopy show the maximum values of $\Delta h/h$ are $O(10^{-3})$ and too small to affect continuity. Therefore, from this point forward, we adopt a rigid lid approximation and assume that $h(x, y) = h =$ constant both outside of and in the interior of the canopy.

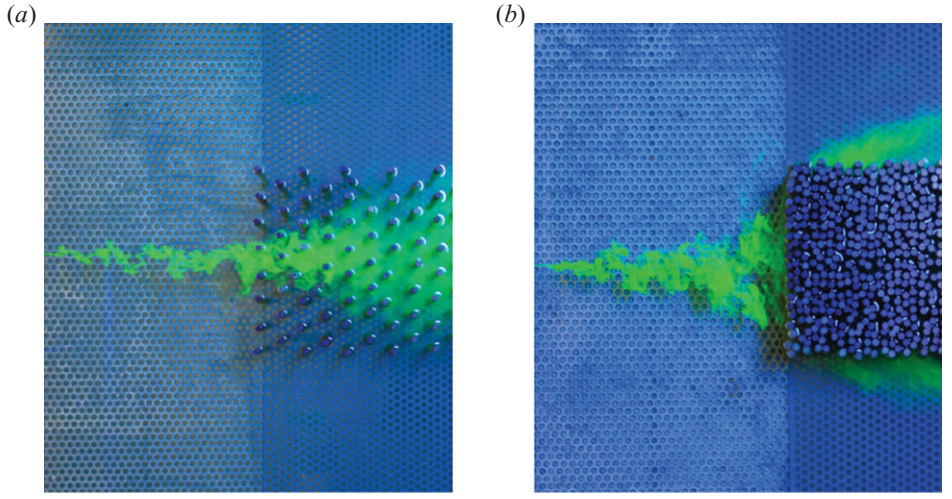

FIGURE 3. Flow at the leading edge of (*a*) a low flow-blockage canopy and (*b*) a high flow-blockage canopy. For the low flow-blockage canopy, the dye trace released at the centreline shows little divergence upstream of the canopy, while for the high flow-blockage canopy, the dye trace diverges significantly upstream of the canopy. Within the low-flow blockage canopy, the spread of the dye trace is primarily due to diffusion.

2.2.2. *Upstream adjustment region*

Far upstream, the flow is assumed to be uniform ($u = U_\infty$ and $v = V_\infty = 0$) and unaffected by the canopy. At the canopy leading edge, there is a step change in the flow resistance with the addition of canopy drag. In aquatic vegetation, canopy drag is generally an order of magnitude or more larger than bed friction. Approaching the leading edge, the fluid begins to decelerate in response to the increase in pressure (see figure 4). The pressure gradient causes lateral flow diversion in a region upstream of the canopy termed the upstream adjustment region (equivalent to the impact region in Belcher *et al.* (2003)). Based on measurements, the lateral divergence of turbulent stress in this region is small and negligible compared to the remaining terms in the momentum equation, and so they are dropped from the momentum equations. Within this region the flow is governed by the following equations of continuity and momentum balance:

$$\frac{\partial \langle \overline{u} \rangle}{\partial x} + \frac{\partial \langle \overline{v} \rangle}{\partial y} = 0, \tag{2.8}$$

$$\langle \overline{u} \rangle \frac{\partial \langle \overline{u} \rangle}{\partial x} + \langle \overline{v} \rangle \frac{\partial \langle \overline{u} \rangle}{\partial y} = -\frac{1}{\rho}\frac{\partial \langle \overline{p} \rangle}{\partial x} - \frac{1}{2}\frac{C_f}{h}\langle \overline{u} \rangle \left(\langle \overline{u} \rangle^2 + \langle \overline{v} \rangle^2 \right)^{1/2}, \tag{2.9}$$

$$\langle \overline{u} \rangle \frac{\partial \langle \overline{v} \rangle}{\partial x} + \langle \overline{v} \rangle \frac{\partial \langle \overline{v} \rangle}{\partial y} = -\frac{1}{\rho}\frac{\partial \langle \overline{p} \rangle}{\partial y} - \frac{1}{2}\frac{C_f}{h}\langle \overline{v} \rangle \left(\langle \overline{u} \rangle^2 + \langle \overline{v} \rangle^2 \right)^{1/2}. \tag{2.10}$$

Although this region is upstream of the porous array, we employ a double average notation for consistency with later equations describing the flow within the array.

Unlike flow near a bluff body, flow can move both through and around a porous array, and the element density plays a role in determining how much of the flow goes through versus around. For low flow-blockage canopies, the streamlines show very little upstream diversion, while for high flow-blockage canopies, the streamlines show significant upstream diversion (figure 3). Within the low flow-blockage canopy,

the spreading of dye is primarily due to turbulent diffusion, rather than divergence, based on the observed velocity field. The visualization shown in figure 3 suggests that high flow-blockage canopies affect upstream flow in a manner similar to bluff bodies, with divergence beginning upstream of the body over a length scale proportional to the canopy width. Therefore, similar to a bluff body, we expect that the pressure increase at the leading edge of high flow-blockage canopies, Δp, scales on ρU_∞^2. In contrast, for low flow-blockage canopies, there is little upstream change in the flow velocity, which implies that the pressure increase at the leading edge is small and that $\Delta p \to 0$ as the canopy flow-blockage approaches zero. The dependence of Δp on the flow-blockage is verified through experimental observations discussed in § 4.

To find the upstream adjustment length, L_O, the governing equations, (2.8)–(2.10), are scaled using the following characteristic values:

$$x \sim L_O, \tag{2.11a}$$

$$y \sim b, \tag{2.11b}$$

$$u \sim U_\infty, \tag{2.11c}$$

$$v \sim \frac{bU_\infty}{L_O} \text{ (from (2.8))}, \tag{2.11d}$$

$$\frac{\partial u}{\partial x} \sim \frac{\Delta u}{L_O}, \tag{2.11e}$$

$$\frac{\partial p}{\partial x} \sim \frac{\Delta p}{L_O}. \tag{2.11f}$$

The scaled governing equations are then

$$\rho \frac{U_\infty \Delta u}{L_O} \sim -\frac{\Delta p}{L_O} - \rho \frac{C_f}{2h(1-\phi)} U_\infty^2 \left[1 + \left(\frac{b}{L_O}\right)^2\right]^{1/2}, \tag{2.12}$$

$$\rho \frac{U_\infty \Delta u}{L_O} \frac{b}{L_O} \sim -\frac{\Delta p}{b} - \rho \frac{C_f}{2h(1-\phi)} U_\infty^2 \frac{b}{L_O} \left[1 + \left(\frac{b}{L_O}\right)^2\right]^{1/2}. \tag{2.13}$$

From these scaled equations we can infer that for all canopies, regardless of the magnitude of the velocity and pressure changes, the pressure and inertial terms balance only if

$$L_O \sim b. \tag{2.14}$$

2.2.3. *Interior adjustment region*

The deceleration that began upstream of the canopy continues within the canopy. However, the retarding force increases due to the addition of canopy drag which is large enough to make bed friction negligible within the canopy. In addition, within the canopy, the double-averaging scheme reveals net stresses due to both spatial and temporal fluctuations. Correlations in instantaneous deviations from the temporal mean produce the Reynolds stress. Correlations in the spatial deviations from the time mean produce a net stress called the dispersive stress. It will be shown in § 4.1 that the Reynolds stress term is negligible compared to the canopy drag term within the flow adjustment region and omitted from the governing equations. The dispersive stress has been shown to be negligible for all but the most sparse canopies ($a < 0.04$ cm^{-1}) and is therefore treated as negligible in this analysis and omitted from the equations (Poggi, Katul & Albertson 2004*a*). The streamwise deceleration

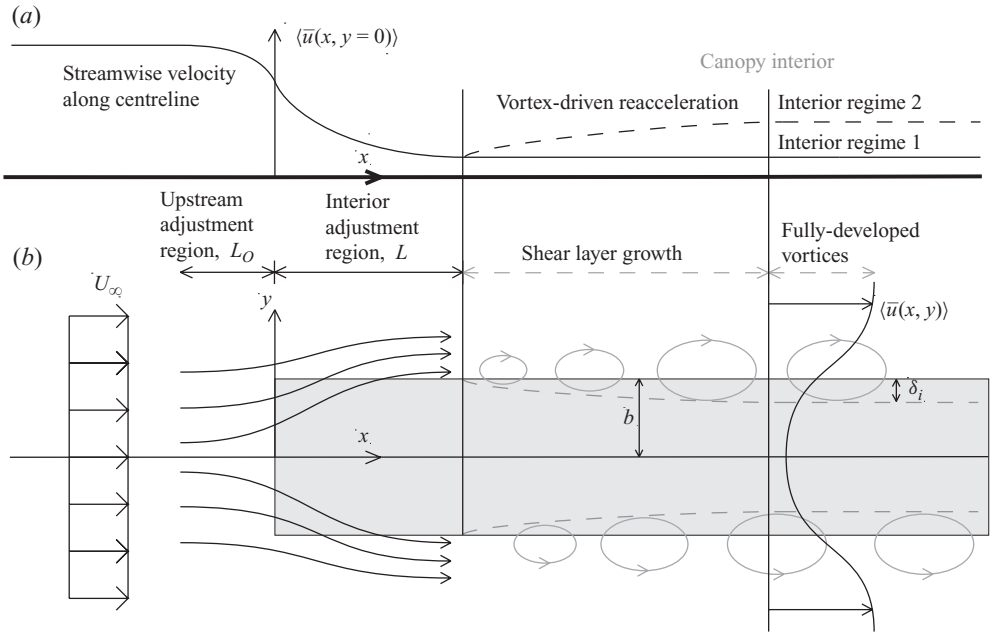

FIGURE 4. (*a*) The streamwise velocity depicted along the canopy centreline. (*b*) Plan view of the flow adjustment at the leading edge of the canopy and the growth of the shear layer and coherent structures along the flow-parallel edges. The flow begins to decelerate upstream of the canopy (upstream adjustment region) and continues to decelerate within the canopy (interior adjustment region). Following the adjustment regions, the flow can enter two different uniform regimes in the canopy interior: (Regime 1) a balance between the pressure gradient and the drag force or (Regime 2) a balance between momentum penetration from the canopy edges and the drag force.

is accompanied by a lateral diversion toward the canopy edges. The deceleration and diversion take place over the length of the interior adjustment region (figure 4). Within this region the flow is governed by the following equations:

$$\langle\overline{u}\rangle\frac{\partial\langle\overline{u}\rangle}{\partial x}+\langle\overline{v}\rangle\frac{\partial\langle\overline{u}\rangle}{\partial y}=-\frac{1}{\rho}\frac{\partial\langle\overline{p}\rangle}{\partial x}-\frac{1}{2}\frac{C_Da}{(1-\phi)}\langle\overline{u}\rangle\left(\langle\overline{u}\rangle^2+\langle\overline{v}\rangle^2\right)^{1/2},\tag{2.15}$$

$$\langle\overline{u}\rangle\frac{\partial\langle\overline{v}\rangle}{\partial x}+\langle\overline{v}\rangle\frac{\partial\langle\overline{v}\rangle}{\partial y}=-\frac{1}{\rho}\frac{\partial\langle\overline{p}\rangle}{\partial y}-\frac{1}{2}\frac{C_Da}{(1-\phi)}\langle\overline{v}\rangle\left(\langle\overline{u}\rangle^2+\langle\overline{v}\rangle^2\right)^{1/2}.\tag{2.16}$$

The final terms in both (2.15) and (2.16) are the spatially averaged drag forces due to the canopy elements in the streamwise and lateral directions, respectively. The drag force is modelled with a quadratic dependence on the mean velocity (Vogel 1994; Koch & Ladd 1997). The drag coefficient, C_D, is a function of the Reynolds number, $Re=\langle\overline{u}\rangle d/\nu$, and the canopy density (Tanino & Nepf 2008).

We scale (2.15) and (2.16) using the characteristic values defined in (2.11), but with L rather than L_O as the unknown streamwise length scale within the canopy and with a dual scaling for the pressure term,

$$\Delta p=0 \text{ (low flow-blockage canopy) or } \rho U_\infty^2 \text{ (high flow-blockage canopy).}\tag{2.17}$$

Dense and sparse canopies	Dense $ab > 0.1$	Canopy contributes sufficient drag to transform velocity profile into a mixing layer form, with inflection point at canopy edge.
	Sparse $ab < 0.1$	Perturbed velocity profile does not contain inflection point.
High and low flow-blockage	High $C_D ab \geqslant 2$	$L \sim b$. Interior velocity driven by pressure gradient
	Low $C_D ab < 2$	$L \sim (C_D a)^{-1}$. Interior velocity driven by turbulent stress

TABLE 1. A summary of the terminology used to categorize porous obstructions in flow.

The scaled equations are

$$\rho \frac{U_\infty^2}{L} \sim -\frac{\Delta p}{L} - \rho \frac{C_D a}{2(1-\phi)} U_\infty^2 \left[1 + \left(\frac{b}{L}\right)^2\right]^{1/2}, \tag{2.18}$$

$$\rho \frac{U_\infty^2}{L}\frac{b}{L} \sim -\frac{\Delta p}{b} - \rho \frac{C_D a}{2(1-\phi)} U_\infty^2 \left[\left(\frac{b}{L}\right)^2 + \left(\frac{b}{L}\right)^4\right]^{1/2}. \tag{2.19}$$

Dividing by the inertial term in each equation, respectively, the equations simplify to

$$1 \sim -\frac{\Delta p}{\rho U_\infty^2} - \frac{1}{2(1-\phi)} \left[(C_D a L)^2 + (C_D ab)^2\right]^{1/2}, \tag{2.20}$$

$$1 \sim -\frac{L^2 \Delta p}{b^2 \rho U_\infty^2} - \frac{1}{2(1-\phi)} \left[(C_D a L)^2 + (C_D ab)^2\right]^{1/2}. \tag{2.21}$$

This form of the scaled equations brings out an important non-dimensional parameter, $C_D ab$, which represents the non-dimensional flow-blockage of the array. The parameter $(C_D a)^{-1}$, called the canopy drag length scale, represents the length scale of flow deceleration associated with canopy drag. The canopy flow-blockage factor is, therefore, a ratio of two length scales: the canopy width, b, and the canopy drag length scale. When this ratio is large, $C_D ab \gg 1$, canopies will be referred to as high flow-blockage canopies, while those with a value of $C_D ab \ll 1$ will be referred to as low flow-blockage canopies (table 1). The transition between these two regimes is expected to occur when $b \approx (C_D a)^{-1}$ or $C_D ab \approx 1$. Measurements described later in the paper suggest that the threshold is closer to 2, i.e. $C_D ab \geqslant 2$ fall in the high flow-blockage regime. We will later show that $C_D ab$ also describes the pressure increase at the leading edge, specifically for high flow-blockage $\Delta p \sim \rho U_\infty^2$ and for low flow-blockage, $\Delta p \to 0$.

Using the dual scaling for the pressure increase at the leading edge (2.17), we can now find the length scale of the interior adjustment region. For low flow-blockage canopies, $C_D ab \ll 1$, and to the first order we assume that $\Delta p = 0$, so that the first and last terms on the right-hand side of (2.20) and (2.21) drop out, indicating $L \sim 2(1-\phi)/C_D a$. However, for these conditions, $\phi \ll 1$, and thus we can simply write

$$L \sim \frac{2}{C_D a}, \tag{2.22}$$

and therefore $L \gg b$. This result is equivalent to that reported by Belcher *et al.* (2003).

For high flow-blockage canopies, $C_D ab \gg 1$ and $\Delta p \sim \rho U_\infty^2$. The pressure term must be $O(1)$ in both equations, which indicates

$$L \sim b \tag{2.23}$$

and therefore $L \gg 2/C_D a$. Taken together, (2.22) and (2.23) imply that L scales on the maximum of $2(C_D a)^{-1}$ and b, a dependence we can capture with

$$L \sim \left[\left(\frac{2}{C_D a}\right)^2 + (b)^2\right]^{1/2}, \tag{2.24}$$

which allows for a smooth transition between the two limits.

2.2.4. *Canopy interior region*

Downstream of the flow adjustment region, $x > L$, the flow can enter two different uniform regimes. In the interior region, the streamlines become parallel to the canopy edges, and the velocity within the canopy is less than the adjacent free stream velocity, creating a shear layer at the canopy's flow-parallel edges (figure 4). When $C_D ab \geqslant 0.1$, the velocity profile in the shear layer exhibits an inflection point (Nepf *et al.* 2007) that is unstable and promotes the growth of Kelvin–Helmholtz vortices (Brown & Roshko 1974; Drazin & Reid 1981; Ho & Huerre 1984; Ghisalberti & Nepf 2002; White & Nepf 2007). Canopies in which $ab < 0.1$ are generally classified as sparse canopies, and those in which $ab > 0.1$ are called dense canopies (Belcher *et al.* 2003; Coceal & Belcher 2004). We are interested in canopies that generate an inflection point in the shear layer, and therefore, with respect to this classification, all of the canopies considered in this analysis are dense. Coherent, Kelvin–Helmholtz vortices have been observed in many experimental settings, including the interfaces of both terrestrial and aquatic canopies (Raupach *et al.* 1996; Tamai, Asaeda & Ikeda 1986; Schatz, Barkley & Swinney 1995). These coherent structures penetrate a distance δ_i into the canopy and dominate mass and momentum exchange in this region. The lateral penetration of coherent structures into a canopy is given by $\delta_i \sim (C_D a)^{-1}$ (Poggi *et al.* 2004*b*; White & Nepf 2007; Nepf *et al.* 2007). The influence of the vortices on the canopy interior depends on how this penetration length scale compares with the transverse dimension of the canopy, i.e. the ratio

$$\frac{\delta_i}{b} \sim \frac{1}{C_D ab}, \tag{2.25}$$

which is the inverse of the canopy flow-blockage factor. When this ratio is small, the canopy interior is isolated from the turbulent stress generated at the canopy edges, and we anticipate that the interior streamwise flow is governed by a balance between the pressure gradient and the canopy drag,

$$0 = -\frac{1}{\rho}\frac{\partial \langle \overline{p} \rangle}{\partial x} - \frac{1}{2}\frac{C_D a}{(1-\phi)}\langle \overline{u} \rangle^2, \tag{2.26}$$

where the lateral velocity, $\langle \overline{v} \rangle = 0$. However, when δ_i is equal to or greater than b, turbulent stress penetrates into the canopy interior and is the dominant driving force for the flow, resulting in a different momentum balance in the interior,

$$0 = -\frac{1}{2}\frac{C_D a}{(1-\phi)}\langle \overline{u} \rangle^2 - \frac{\partial}{\partial y}\left(\langle \overline{u'v'} \rangle\right), \tag{2.27}$$

where $-\rho\langle \overline{u'v'} \rangle$ is the Reynolds stress. The following scale analysis indicates that the pressure gradient is negligible in this interior regime. If the vortices penetrate to the

centre of the canopy, the Reynolds stress term will scale as

$$\frac{\partial}{\partial y}\left(\langle\overline{u'v'}\rangle\right) \sim \frac{U_\infty^2}{b}. \tag{2.28}$$

Because the uniform upstream velocity is set by the balance between the pressure gradient and bed drag, we can also write

$$\frac{1}{\rho}\frac{\partial p}{\partial x} = \frac{C_f}{h}U_\infty^2. \tag{2.29}$$

Combining (2.28) and (2.29), the ratio of the Reynolds stress term to the pressure term is h/bC_f, which is large (>50) for every experiment in this study, confirming that when the vortices penetrate to the canopy centreline, the Reynolds stress gradient dominates over the pressure gradient and (2.27) applies.

Belcher *et al.* (2003) also defines submerged canopies as shallow or deep based on the ratio of the canopy height, defined h_e in that work, and the penetration of the shear layer into the canopy. If the two length scales are comparable, the canopy is shallow, and if the canopy height is much greater than the penetration length of the shear layer, the canopy is deep. Using the fact that the penetration of the shear layer into the canopy scales on $(C_Da)^{-1}$ and drawing on the geometric parallel between the canopy height in submerged canopies, h_e, and the canopy width in shallow water canopies, b, it is evident that the definitions shallow and deep are similar to the definitions of low and high flow-blockage. Therefore, the canopy flow-blockage factor, C_Dab, governs both the length scale of the flow adjustment regions (2.24), and the influence that the turbulent stresses have on the interior velocity, downstream of the adjustment regions. Experiments described below suggest that the transition between high and low flow-blockage occurs near a threshold value of $C_Dab = 2$. To summarize, high flow-blockage canopies, where $C_Dab \geqslant 2$, have an interior adjustment length proportional to the canopy width, b, and an interior velocity driven by the ambient pressure gradient, while low flow-blockage canopies, $C_Dab < 2$, have an interior adjustment length proportional to the canopy drag length scale, $(C_Da)^{-1}$, and an interior velocity driven by the lateral gradient in the turbulent stress. This scaling and the transition between low flow-blockage and high flow-blockage canopies will be tested and discussed in § 4.

3. Methods

Experiments were conducted in the Environmental Fluid Mechanics Laboratory at MIT in a 13 m long, 1.2 m wide recirculating flume. In this flume, a 25 hp pump draws water from the tailbox and pumps it upstream to the headbox, where a large baffle helps disperse the flow evenly across the flume width. A weir at the downstream end of the test section sets the flow depth.

Several different model canopies were constructed and tested in this flume. The canopies were placed at mid-channel and 6 m from the flume outlet. The canopies were constructed of maple dowels, 6.4 mm in diameter and 15 cm high, in a flow of depth $h = 14$ cm. The dowels were arranged in rectangular canopies in perforated PVC boards which lined the flume bed. The two parameters of canopy geometry that were varied were the half-width, b, and the density, a. The density was varied between $\phi = 2.6$ % and 40 %, or $a = 0.053$–0.8 cm^{-1}. The canopy half-width was varied between $b = 4$ and 13 cm. The corresponding range of flow-blockage was $C_Dab = 0.2$–8.0, which covers many field canopies (table 2). For example, kelp forests have values

C_Dab	a (cm^{-1})	b (cm)	ϕ(%)
0.21	0.053	4	2.6
0.53	0.053	10	2.6
0.58	0.096	6	4.6
0.96	0.096	10	4.6
1.2	0.20	6	10.3
1.25	0.096	13	4.6
2.0	0.20	10	10.3
3.0	0.20	15	10.3
4.8	0.80	6	40
8.0	0.80	10	40
8.0*	0.20	40	10.3

TABLE 2. The parameters of 12 experimental canopies. The densities were dictated by the board hole spacings. The asterisk (*) indicates a velocity profile measured by Zong and reported in Zong & Nepf (2010). Although the drag coefficient varies with velocity over the length of the array, it was defined as $C_D = 1$ in the table.

of $C_Dab \approx 0.5$–30, based on parameters reported by Jackson (1997), Rosman *et al.* (2007) and Gaylord *et al.* (2007). Luhar *et al.* (2010) reports values of C_Dab between 1 and 15 for seagrasses in the coastal ocean. Bouma *et al.* (2007) constructed model marshgrass canopies of $C_Dab = 0.19$ and 3.1, which are representative of naturally occurring canopies of emergent aquatic vegetation. Finnigan (2000) reports values of $C_Dab = 0.2$–1.5 for agricultural canopies, and $C_Dab = 1$–5 for terrestrial forests (note that for terrestrial canopies, b is the canopy height). Large urban areas typically have values of C_Dab between 0.1 and 0.3 (Grimmond & Oke 1999). In all of these reported ranges of C_Dab, C_D is assumed to be unity. In our experiments, to minimize the influence of the flume walls, the canopy width was never larger than 26 cm, or $\approx 20\,\%$ of the total flume width. The canopy length was not a parameter expected to influence the flow adjustment region, provided that the overall canopy length was much larger than the adjustment length. The flowrate was held constant with a uniform approach velocity of $U_\infty \approx 10$ cm s^{-1} for all experiments.

Velocities were measured along the x-axis upstream of the canopy and within the canopy using a 3D Nortek Vectrino acoustic Doppler velocimeter (ADV). The sampling volume of the ADV was located at mid-depth in the flow. At each point, the three velocity components (u,v,w) were recorded at 25 Hz for 240 s. Upstream of the canopy, velocities were measured at 10 cm intervals, starting between $x = -150$ and -100 cm. Within the canopy, velocities were measured at intervals proportional to the expected adjustment length of the individual canopy. For example, for a canopy with a longer adjustment length, velocities were measured at intervals of 10 cm or greater. For a canopy with a shorter adjustment length, measurements were taken at intervals of between 3 and 5 cm. Within the canopies, the exact sample spacing was determined by the dowel geometry and spacing.

At all of the sampling points, the ADV was placed in the same orientation relative to the surrounding dowels. Consistency in placement and orientation was critical to minimize the error introduced by spatial heterogeneity in the velocity through the dowel array. The sampling volume was positioned as close as possible to the midpoint between two dowels. The velocity at this position has been shown to be within 20 % of the spatially averaged velocity, $\langle\overline{u}\rangle$, for all of the array densities investigated here (White & Nepf 2003). The error due to velocity variations in time was negligible due

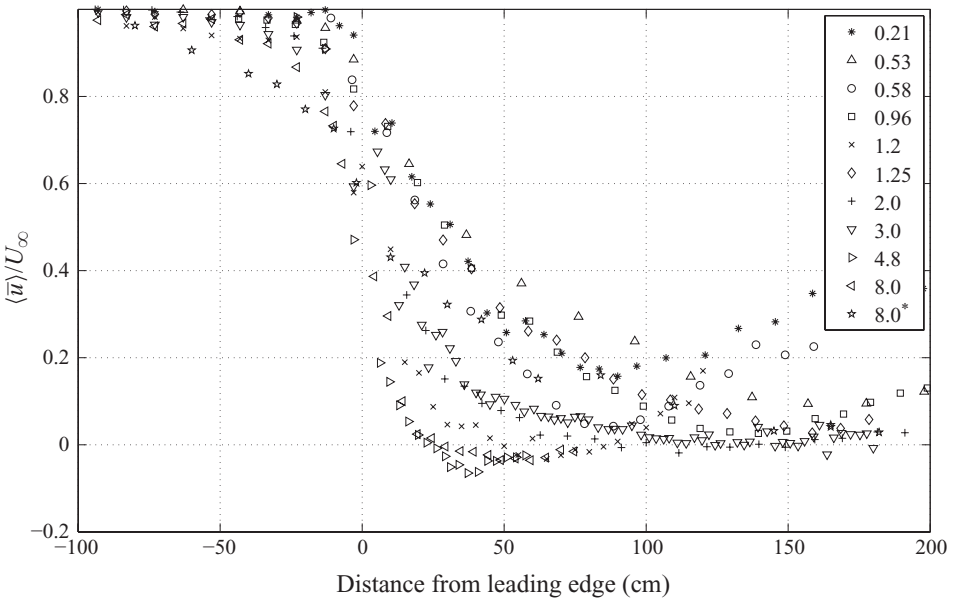

FIGURE 5. The streamwise velocity profiles along the canopy centreline, starting upstream of the canopies and through the length of the adjustment region. The canopies begin at $x = 0$. The streamwise velocity $\langle\overline{u}\rangle$ has been normalized by the upstream velocity U_∞.

to the large number of data points. Within the canopies of density $a \geqslant 0.2$ cm^{-1}, it was necessary to remove a few individual dowels to fit the head of the ADV probe into the canopy. The ADV sampling volume is 6 mm in diameter, 2.5 mm in height and is located 7 cm below the probe head of the ADV. The instrument is designed to produce minimal local distortion in the sampling volume.

At intervals of 10 cm along the canopy edges, two capacitance-based wave gauges were used to monitor the displacement of the water surface. The displacement was recorded at 25 Hz for 240 s and was filtered to remove high-frequency noise. The Kelvin–Helmholtz vortices create a small dimple in the water surface, which appears as a small negative displacement. The filtered surface displacement signals are then used to deduce the phase and period of the passing vortices.

Velocity profiles were also measured in the cross-stream direction for selected canopies in the fully developed region of the flow (figure 4). The measurements were taken at intervals of between 2 and 4 cm starting at the canopy centrelines and continuing into the free stream. To investigate the interaction between vortices on the two flow-parallel edges, a second set of cross-stream velocity profiles were taken with a thin splitter plate in place at the canopy centreline. This splitter plate prohibited communication between the vortices at the two canopy edges.

4. Results and discussion

4.1. *Flow adjustment regions*

The streamwise velocity profiles exhibit a range of behaviour both upstream of and within the canopy (figure 5). We first consider the upstream adjustment region and define the upstream velocity change as $\Delta u = U_\infty - u_{(x=0)}$. The upstream adjustment length, L_O, was defined as the distance over which 90 % of this velocity change occurred, i.e. the upstream adjustment region begins at the point where

$u = u_{(x=0)} + 0.9\Delta u$. This definition was chosen to remove the biases associated with the magnitude of the velocity drop. The scaling of the governing equations suggests that for both high and low flow-blockage canopies, $L_O \sim b$. The observations support this scaling even though the upstream deceleration is weaker for sparser canopies. Across all of the canopies, $L_O = (4.0 \pm 0.7)b$, with no dependence on $C_D ab$, where the uncertainty is the standard error of the normalized, measured values.

In the canopies with the highest solid volume fractions, a flow reversal is observed within the canopy and near the leading edge (figure 5). In these canopies, the upstream flow divergence is so strong that the velocity at the two leading-edge corners ($x = 0$, $y = \pm b$) is elevated above the free-stream velocity (see details in figure 4 of Zong & Nepf (2010)) such that a low pressure zone is created at these corners. For flow around solid obstructions, a similar local pressure is associated with flow separation. In the porous arrays studied here, this local adverse pressure gradient is sufficient, relative to the low inertia of the flow within the canopy, to cause a flow reversal within the canopy. This phenomenon has also been observed in dense terrestrial canopies (Krzikalla 2005). A flow reversal was observed for two high flow-blockage cases, $C_D ab = 4.8$ (▷) and 8.0 (◁), which were also the narrowest canopies, $b = 6$ and 10 cm, respectively (see $\langle \overline{u} \rangle < 0$ at $x \approx 40$ cm in figure 5). In wider canopies, flow reversals may also be present, but may be found closer to the corners and not at the centreline, where our profiles are made.

We can use the measured velocity profiles to examine the magnitude of the pressure change, Δp, at the leading edge and to confirm the scaling proposed in § 2.2.3. For bluff bodies, the pressure at the stagnation point is proportional to the kinetic energy of the flow upstream, $1/2\rho U_\infty^2$. We anticipate that canopies with high values of $C_D ab$ will approach this limit, but canopies with a value of $C_D ab \to 0$ will experience a negligible elevation of pressure, $\Delta p \to 0$. According to Bernoulli, we can define the scale of the pressure change using the change in kinetic energy between a position far upstream and at the leading edge,

$$\frac{\Delta p}{\rho U_\infty^2} \sim \frac{\rho U_\infty^2 - \rho \langle \overline{u} \rangle_{x=0}^2}{\rho U_\infty^2}. \tag{4.1}$$

When this value is a constant close to unity, it is reasonable to define the pressure change at the leading edge as $\Delta p \sim \rho U_\infty^2$. This scaling for Δp is valid for $C_D ab > 2$ (figure 6). For values of $C_D ab < 2$, the data shown in figure 6 suggest that $\Delta p / \rho U_\infty^2$ increases with $C_D ab$ and that $\Delta p \to 0$ for $C_D ab \to 0$. These results support the assumption of a dual scaling for the pressure as represented in (2.17).

Within the canopy, the interior adjustment length is estimated from the data as the point downstream of the leading edge at which the velocity reaches a minimum or constant value. The measured interior adjustment length is the shortest for narrow and dense canopies and is the longest for wide and sparse canopies (figure 5). For example, the canopy with $b = 6$ cm and $a = 0.8$ cm^{-1} ($C_D ab = 4.8$, ▷) has an interior adjustment length of 30 cm, while the canopy with $b = 10$ cm and $a = 0.053$ cm^{-1} ($C_D ab = 0.53$, △) has an interior adjustment length of 150 cm. By normalizing the x-coordinates by the length scale of the interior adjustment region, L, as given in (2.24), the streamwise velocity profiles collapse, confirming the scaling argument derived in § 2.2.3. (figure 7). The mean and the standard error of the measured adjustment lengths provide the scale constant for (2.24), specifically

$$L = (5.5 \pm 0.4)\left[\left(\frac{2}{C_D a}\right)^2 + (b)^2\right]^{1/2}. \tag{4.2}$$

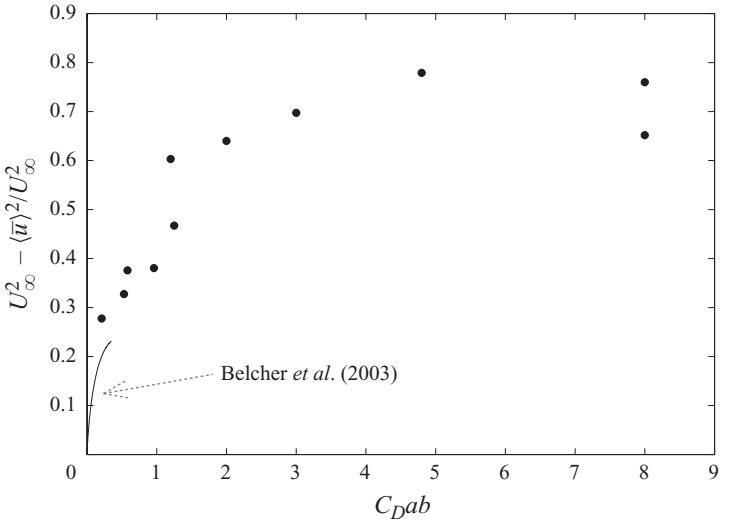

FIGURE 6. The measured kinetic energy change at the leading edge of the canopy for the full range of values of $C_D ab$. The prediction of Belcher *et al.* (2003), valid only for canopies with very low flow-blockage, $C_D ab \ll 1$, is plotted with a solid line.

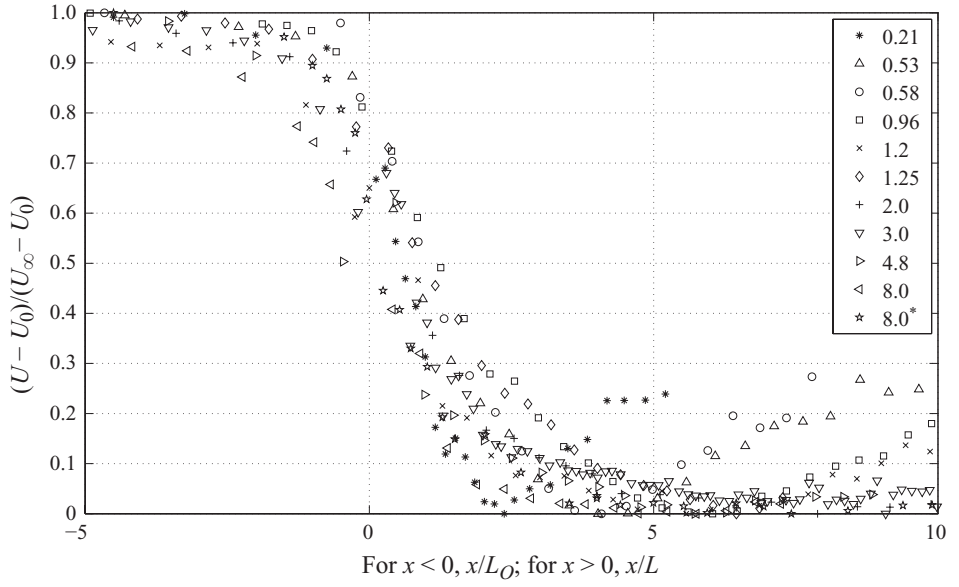

FIGURE 7. The streamwise velocity profiles along the centreline, normalized by the length scale (2.24) predicted from scaling the governing equations. Within the canopy, L is given by (2.24). Upstream of the canopy, the velocity profiles are normalized by L_O, which is given by (2.14). The velocity has been normalized by the difference between the upstream velocity, $U\infty$, and the minimum velocity at the end of the flow adjustment region, U_0.

The drag coefficient, C_D, was set equal to unity for simplicity. For low flow-blockage canopies, for which L reduces to $L \sim (C_D a)^{-1}$, this result is in agreement with the adjustment length scale of Coceal & Belcher (2004).

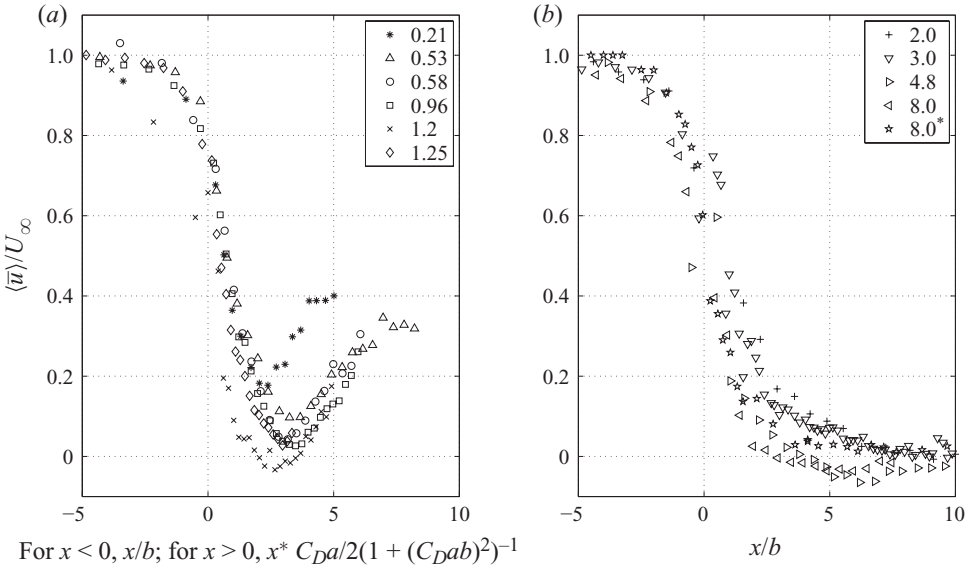

FIGURE 8. The streamwise velocity profiles along the centreline. (*a*) Low flow-blockage canopies normalized by (4.3) within the canopy and by (2.23) upstream of the canopy. The values of $2/C_D a$ range from 10 to 38 cm (table 2). (*b*) High flow-blockage canopies normalized by (2.23). The values of b range from 6 to 40 cm (table 2).

Drawing on the work of Belcher *et al.* (2003), we can add a correction term to the scaling that accounts for the small, but non-zero, pressure change at the leading edge of low flow-blockage canopies. For sparse canopies, $ab<0.1$, Belcher *et al.* (2003) found the velocity deficit at the canopy leading edge to be proportional to $C_D ab$. This scaling is shown as a solid line in figure 6. Utilizing this result, we can define the pressure change $\Delta p/\rho U_\infty^2 \sim (C_D ab)^2$. Thus for low flow-blockage canopies, the interior adjustment length with the small correction term is

$$L \sim \frac{2}{C_D a}\left(1+(C_D ab)^2\right). \tag{4.3}$$

In figure 8, the data are separated into two different sets, low flow-blockage and high flow-blockage, and compared against the appropriate scaling, either (4.3) or (2.23). Based on the scaling (2.24) and the data in figure 6, the transition between low and high flow-blockage is expected to occur at $C_D ab=2$, and this is the threshold used to separate the cases in figure 8. This figure shows more clearly how the higher values of $C_D ab$ scale with canopy width, b, and how lower values of $C_D ab$ scale with the canopy drag length scale. Further, note that all of the low flow-blockage canopies exhibit the same flow reacceleration behaviour downstream of the adjustment regions. In the low flow-blockage canopies, the refined adjustment length (4.3) is found to be

$$L=(3.0\pm0.3)\left[\frac{2}{C_D a}\left(1+(C_D ab)^2\right)\right]. \tag{4.4}$$

This scale constant is consistent with the observations reported in Coceal & Belcher (2004), who find $L=3L_c$, with $L_c=2(1-\phi)/(C_D a)$, where $\phi\ll1$ for low flow-blockage canopies. In the high flow-blockage canopies, the adjustment length is found to be

$$L=(7.0\pm0.4)b. \tag{4.5}$$

In the results for both low and high flow-blockage canopies, the uncertainty reported is the standard error of the normalized, measured adjustment lengths.

Belcher, Finnigan & Harman (2008) reports that both the upstream and interior adjustment regions in low flow-blockage canopies scale on $(C_D a)^{-1}$. Our observations do not support this conclusion. While we find that the interior adjustment region of canopies with low flow-blockage scales on $(C_D a)^{-1}$, the measurements and scale analysis indicate that the upstream adjustment region scales on the canopy width, b. In high flow-blockage canopies, our scaling analysis indicates that both the upstream and interior adjustment regions share the same length scale, the canopy width b, and the results support this conclusion. All of the canopies tested in this paper are considered dense ($C_D ab \geqslant 0.1$) using the terminology of Belcher *et al.* (2003) and Coceal & Belcher (2004). Canopies with very low flow-blockage ($C_D ab \leqslant 0.1$), i.e. sparse canopies, were not tested in this study and may exhibit different behaviour.

The spread that remains in the normalized data (figure 7) can be attributed to several factors. First, the half-width of a uniform, staggered array is not clear, particularly for sparse arrays, as there is a staggered interface between the free stream and the canopy. Second, there is uncertainty in the drag coefficient, C_D, which is described by empirical formulas as a function of ϕ and velocity and based on uniform flow conditions. Finally, spatial error in the velocity profiles can also influence the adjustment region. Although point measurements were taken with constant geometric positioning with respect to the surrounding canopy elements, spatial deviations from the mean velocity exist, and finer scale measurements would be unattainable within dense canopies.

For the flow within the canopies to decelerate, fluid must be diverted laterally across a distance b to the canopy edges. The laterally moving flow also experiences a drag force (the last term in (2.16)). For high flow-blockage canopies, $L \sim b$, (2.11*d*) indicates that $v \sim u$, and therefore the flow resistance in the lateral direction is comparable to the streamwise flow resistance and provides an equal control on the flow. That is for high flow-blockage canopies, the streamwise flow can adjust only as rapidly as fluid can laterally evacuate the canopy interior. This is why the canopy width is the controlling length scale of flow adjustment. In contrast, for canopies with low values of $C_D ab$, $L \gg b$ and $v \ll u$, and the lateral flow resistance is small compared to the streamwise flow resistance. Fluid is able to evacuate the canopy interior with negligible constraint on the lateral flow, and therefore the interior flow adjustment length scale depends on the canopy drag, with very little dependence on the canopy width. For canopies that fall in the transition region between these two distinct regimes, the adjustment length is controlled by a combination of the canopy width and the canopy drag (4.2).

It was assumed *a priori* that within the adjustment region there is a negligible contribution from turbulent stress and that the governing equations for the flow reduced to (2.15) and (2.16). The experimental measurements confirmed this showing the Reynolds stress gradient was negligible within the region of streamwise velocity deceleration. For this scaling analysis, the Reynolds stress gradient at the centreline of the canopy is approximated as

$$\left.\frac{\partial \langle \overline{u'v'} \rangle}{\partial y}\right|_{y=0} \approx \frac{\langle \overline{u'v'} \rangle_{y=b}}{b}. \tag{4.6}$$

Note that this estimate is quantitatively accurate when $\delta_i \geqslant b$, indicating stress can penetrate to the centreline. Otherwise, (4.6) overestimates the stress gradient at the centreline. First-order, forward differences were used to approximate the inertial term.

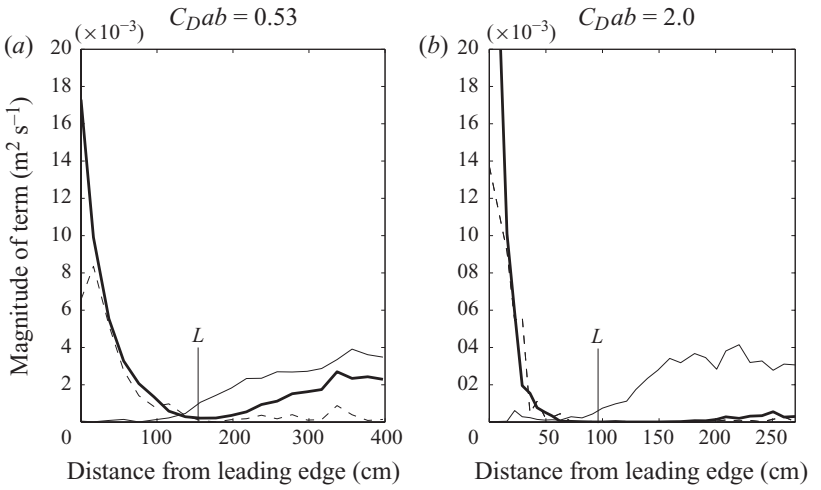

FIGURE 9. Magnitudes of the inertial term (dashed line), the Reynolds stress term (thin solid line) and the canopy drag term (heavy solid line) in the momentum equation. The inertial term shows non-zero values during the adjustment region. For the low flow-blockage canopy, $C_Dab = 0.53$, the Reynolds stress term becomes significant beyond the interior adjustment region and is balanced by the canopy drag term. For the high flow-blockage canopy, $C_Dab = 2.0$, the Reynolds stress does not penetrate to the centreline and the force balance is between the pressure gradient and canopy drag. The adjustment length, L, is denoted on the x-axis.

The estimated magnitudes of the inertial, stress and drag terms are shown in figure 9 for a high and low flow-blockage case. The inertial term (dashed line) of the momentum equation has non-zero values in the interior flow adjustment region ($x < L$), where it is balanced by canopy drag. As assumed, the Reynolds stress term (thin, solid line) is negligible within the interior adjustment region. Downstream of the interior adjustment region, $x > L$, the inertial terms drop to zero. In the low flow-blockage canopy ($C_Dab = 0.53$, figure 9*a*), the Reynolds stress and drag terms are in balance. In the high flow-blockage canopy (figure 9*b*), $\delta_i < b$, such that (4.6) is an overestimate of the turbulent stress gradient at the centreline. Indeed, this estimator is clearly out of balance with the drag term in figure 9. The relevant force balance is then between the canopy drag and the pressure gradient. These two regimes of interior flow are discussed further in the next section. Measurements of the lateral divergence of the Reynolds stress show that this term is negligible in comparison to the inertial terms upstream of the array as well.

4.2. *The shear layer and canopy interior regions*

In figure 8, the velocity profiles were separated based on their values of C_Dab. The canopies with low flow-blockage ($C_Dab < 2$) all show a clear reacceleration after the adjustment region, while this behaviour is absent in the high flow-blockage canopy profiles. Two specific streamwise velocity profiles are shown in figure 10 for a representative high flow-blockage and low flow-blockage canopy. For the low flow-blockage canopy, $C_Dab = 0.53$, the streamwise velocity reaccelerates after the flow adjustment regions and approaches a uniform interior flow velocity which is set by the balance of turbulent stress penetrating to the canopy interior and canopy drag, as suggested by (2.27).

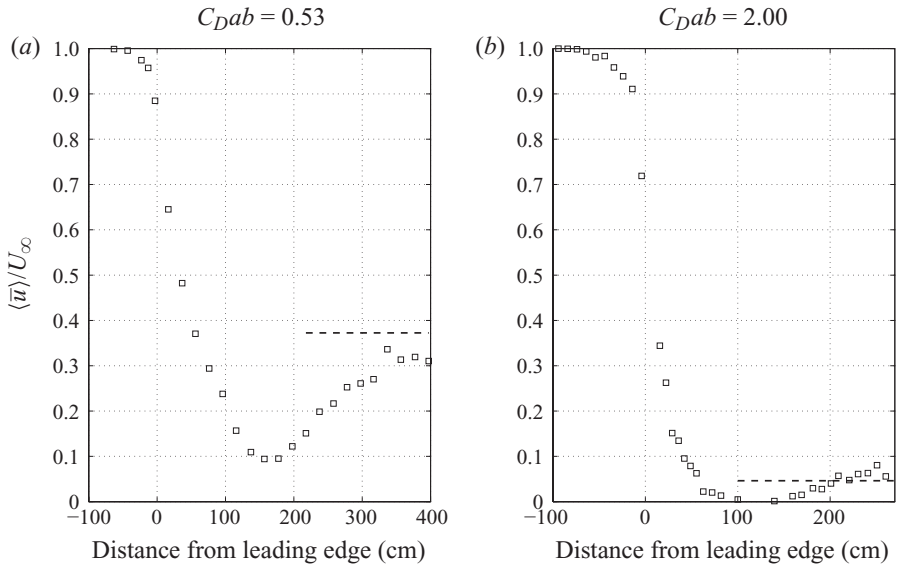

FIGURE 10. The streamwise velocity profiles through the interior adjustment region and the canopy interior. (*a*) In the low flow-blockage canopy, $C_Dab = 0.53$, re-acceleration occurs beyond the initial adjustment region, and the interior velocity is set by a balance of turbulent stress penetration and canopy drag. The prediction (4.8) is shown by the dashed line. (*b*) In the high flow-blockage canopy, $C_Dab = 2.0$, the interior velocity is set by a balance of the pressure gradient and canopy drag. The prediction (4.10) is plotted with the dashed line.

Using the estimator of the turbulent stress gradient shown in (4.6) and the definition,

$$u_* = \sqrt{-\langle\overline{u'v'}\rangle_{y=b}}, \tag{4.7}$$

the interior velocity of low flow-blockage canopies given by (2.27) can be written as

$$\frac{\langle\overline{u}\rangle}{U_\infty} = \frac{1}{U_\infty}\sqrt{-\frac{\partial}{\partial y}\left(\langle\overline{u'v'}\rangle\right)\frac{2(1-\phi)}{C_Da}} = \frac{1}{U_\infty}\sqrt{\frac{u_*^2}{b}\frac{2(1-\phi)}{C_Da}}. \tag{4.8}$$

Using $C_D = 1$, (4.8) closely predicts the interior velocity of the low flow-blockage canopy (shown as dashed line in figure 10*a*). If measurements of u_* are not available, previous researchers have predicted the strength of the turbulent stress based on canopy morphology and the free stream velocity profile (Bentham & Britter 2003; Belcher *et al.* 2003).

For the high flow-blockage canopy of $C_Dab = 2$, the uniform interior velocity is set by a balance between the pressure gradient and canopy drag, derived from (2.26),

$$\langle\overline{u}\rangle = \sqrt{-\frac{2}{\rho}\frac{\partial p}{\partial x}\frac{(1-\phi)}{C_Da}}. \tag{4.9}$$

The background pressure gradient can be estimated from the momentum balance in the free stream, i.e. the balance between bed friction and the pressure gradient shown in (2.29). Then, (4.9) can be written as

$$\frac{\langle\overline{u}\rangle}{U_\infty} = \sqrt{\frac{C_f}{h}\frac{(1-\phi)}{C_Da}}. \tag{4.10}$$

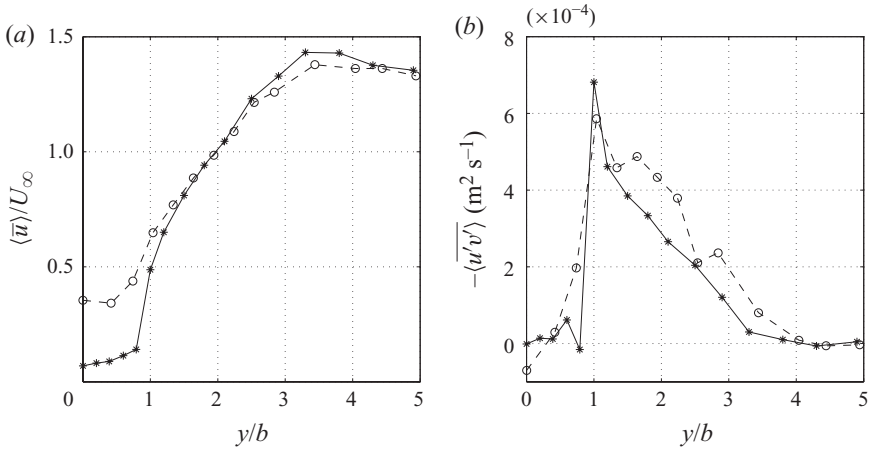

FIGURE 11. The cross-stream profiles of (*a*) streamwise velocity and (*b*) Reynolds stress profiles in the fully developed region of the flow for $C_D ab = 0.53$ (○, dashed line) and 2.0 (*, solid line). The profiles were measured at streamwise distances of $x = 360$ and 262 cm, respectively. The canopy centreline is at $y/b = 0$, and the canopy edge is at $y/b = 1$. The error in the velocity data is $\pm$ 0.0025 m s^{-1} within the canopy and is negligible in the free stream ($y/b > 1$). The error in the Reynolds stress is 4×10^{-5} m^2 s^{-2} within the canopy and is negligible in the free stream.

The interior flow velocity was predicted from (4.10) using the known coefficient of friction for the PVC baseboards, $C_f = 0.006$ and C_D was set equal to unity. The prediction, shown with the dashed line in figure 10(*b*), is in agreement with the observed velocity, confirming the force balance suggested in (2.26). The near reversal in the streamwise velocity at $x = 100$ cm for $C_D ab = 2.0$ is likely associated with the high velocity/low pressure region at the leading corners, which was discussed previously in § 4.1.

Figure 11 shows the lateral profiles of the mean streamwise velocity and Reynolds stress in the fully developed region of the two canopies described in figures 9 and 10. Note that figure 11 shows the stress profile over only half the canopy. The outer layer, which is the portion of the shear layer in the free stream is similar in scale for both canopies because it is set by h/C_f (White & Nepf 2007). The inner shear layer scale, or penetration scale, is $\delta_i/b = 0.5/(C_D ab)$ (White & Nepf 2007). When $C_D ab = 2.0$, $\delta_i/b \approx 0.25$ and turbulent stress does not penetrate to the canopy interior. The experimental results show that the Reynolds stress is essentially zero, within uncertainty, over the span from the centreline, $y/b = 0$, to near the edge, $y/b \approx 0.8$, so that the gradient equals zero at the centreline. For these conditions, the mean streamwise velocity at the centreline is driven by the pressure gradient (2.26), as shown in figure 10(*b*). For $C_D ab = 0.53$, $\delta_i/b \approx 1$ and the stress profile is approximately linear from one canopy edge to the other, passing through zero near the canopy centreline, consistent with the change in velocity gradient at the centreline. Based on the measured stress profile, $\partial\langle\overline{u'v'}\rangle/\partial y = 0.0024$ m s^{-2} at the centreline, which is comparable to the estimator used previously, $\langle\overline{u'v'}\rangle_{y=b}/b = 0.0040$ m s^{-2}. For this canopy ($C_D ab = 0.53$), the streamwise velocity increases after the flow adjustment region (figure 10*a*) because turbulent stress can penetrate to the canopy interior, and the streamwise velocity at the centreline is set by the balance of turbulent stress and drag (2.27).

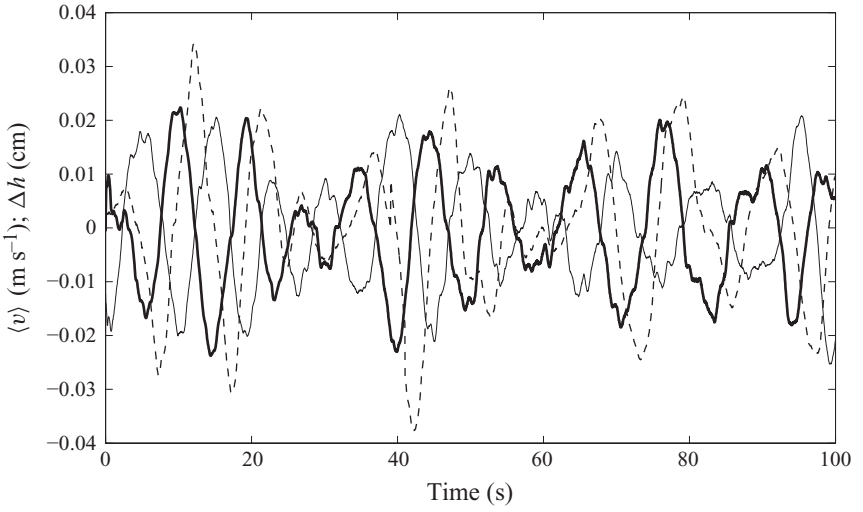

FIGURE 12. A time record of the surface displacement, Δh, just outside of the canopy edges ($x = 160$ cm, $y = 13$ cm, thin solid line; $y = -13$ cm, heavy solid line) as well as the response of the instantaneous in-canopy lateral velocity, $\langle v \rangle$ (dashed line), in the fully developed region of the canopy of $C_D ab = 0.53$. The surface displacements show a phase shift of π radians while the velocity lags the low-pressure events by $\pi/2$ radians.

4.3. *Vortex organization and enhancement*

Studies of canopies with a single flow-parallel edge have shown that the Kelvin–Helmholtz vortices induce a pressure response beyond the scale of the vortex (Finnigan & Shaw 2000; White & Nepf 2007). The centre of each vortex is a point of low pressure which induces a wave response in the array beyond the penetration length, δ_i. In this study, the canopy has two streamwise interfaces separated by the full canopy width, $B = 2b$ (figure 1). The time records of the surface displacement at the canopy edges suggest that the vortices interact across the canopy width. Specifically, the vortices organize such that there is a phase shift of π radians between the vortex streets that form on either side of the canopy (figure 12). The resulting cross-canopy pressure gradient induces a transverse velocity (v) within the canopy that lags the pressure forcing by $\pi/2$ radians (figure 12).

The vortex pattern evolves from the leading edge as shown diagrammatically in figure 4. Figure 13 provides evidence that travelling vortices appear at $x = 50$ cm, which is near the end of the adjustment region, $x = L$. Upstream of $x = L$, the flow is diverting laterally and the shear layer has not yet formed. Once formed, the vortices quickly organize, such that by $x = 100$ cm, there is a phase shift of π radians between the vortex streets on either side of the canopy, which is evident in the cross-canopy lag of $1/2$ of the vortex period (figure 13).

The communication of vortices across the canopy not only results in self-organization, but also in a significant enhancement of the strength of the vortices. The strength of the vortices can be described by the magnitude of the peak Reynolds stress. This magnitude was compared for conditions in which the vortices were able to communicate across the canopy, and conditions in which this communication was blocked by a splitter plate placed at the canopy centreline. For both the low and high flow-blockage canopies, there is a significant enhancement in stress at the interface when vortices can communicate across the canopy (no splitter plate). For

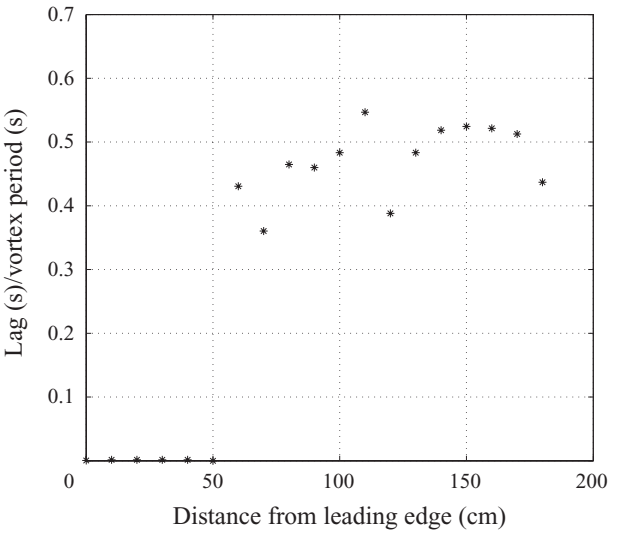

FIGURE 13. The shift between the surface displacement at the two canopy edges for $C_D ab = 3.0$, in seconds, normalized by the measured instability period. The normalized phase shift converges to a value 0.5 downstream of the leading edge, indicating that the two canopy edges are perfectly out of phase. Near the leading edge, vortices have not yet formed and the turbulence is of a random nature and therefore the two signals are uncorrelated.

$C_D ab = 0.53$, the vortices penetrate the full half-width into the canopy, $\delta_i / b \approx 1$, and the Reynolds stress increases by nearly a factor of 5 between cases with and without the splitter plate. For $C_D ab = 2$, the vortices penetrate a very small distance into the canopy, $\delta_i / b \approx 0.25$, and yet the Reynolds stress at the edge increases by a factor of 7.

The cross-canopy organization of vortices greatly enhanced the lateral transport of fluid across the canopies. This was most evident in the root mean square of the lateral velocity, v_{rms}, in the canopy interior (figure 14). Within the low flow-blockage canopy, $C_D ab = 0.53$, v_{rms} approaches 3 cm s^{-1}. Using half the period of a passing vortex as the representative time scale, the excursion amplitude is approximately 17 cm, a distance greater than the half-width of the canopy of 10 cm. Within the high flow-blockage canopy, $C_D ab = 2.0$, v_{rms} approaches 2.5 cm s^{-1} and results in an excursion amplitude of 14 cm, which is also comparable to the canopy half-width, $b = 10$ cm. That is, despite a much smaller penetration length in the high flow-blockage canopy, $\delta_i \approx 2.5$ cm, the cross-canopy velocity response to vortex passage has nearly the same amplitude as that observed in the low flow-blockage canopy. These results indicate that fluid parcels in the centre of both the low and high flow-blockage canopies containing spores, nutrients, pollution or small creatures can be drawn into the free stream and vice versa, over half the period of a single passing vortex.

In a one-sided canopy, or a canopy with a splitter plate at the centreline (figure 14), v_{rms} is reduced over the entire canopy width and necessarily approaches zero at the centreline. This reveals that two-sided canopies not only produce much stronger vortices, but that their retention time can be influenced more strongly by the lateral response to passing vortices. Indeed, in the two-edge canopies, v_{rms} has nearly the same magnitude as $\langle \overline{u} \rangle$ in the low flow-blockage canopy, while v_{rms} is larger than $\langle \overline{u} \rangle$ in the high flow-blockage canopy (figures 11 and 14). This result suggests that lateral motions, rather than streamwise advection, can control the canopy residence

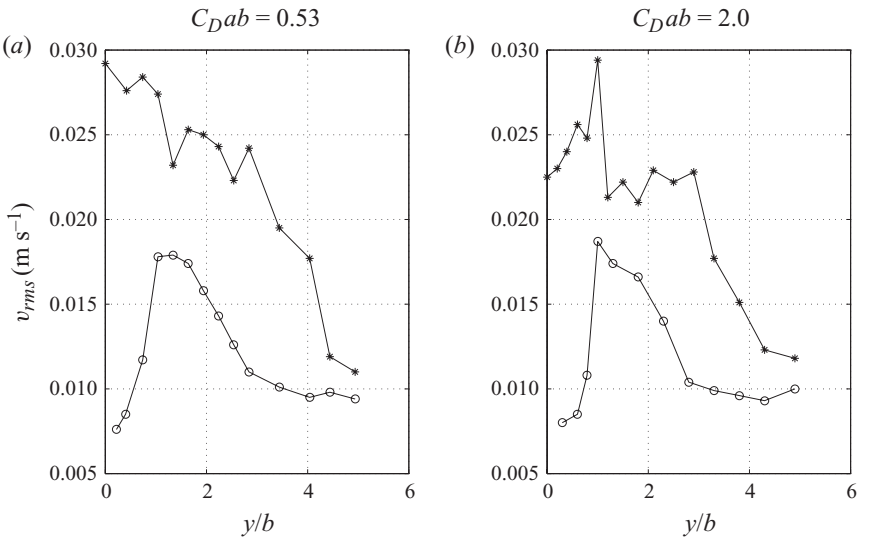

FIGURE 14. The lateral, root-mean-square velocity, v_{rms} shown for both canopy densities with ($\circ$) and without ($*$) a splitter plate at the canopy centreline. The values of v_{rms} are greatly reduced in the presence of the splitter plate and approach zero at the canopy centreline, $y/b = 0$. The error in the velocity data is $\pm$ 0.0025 m s^{-1} within the canopy ($y/b \leqslant 1$) and is negligible in the free stream ($y/b > 1$).

time. This is especially true when the aspect ratio of the canopy is greater than one, which is typical in channel vegetation, e.g. Sand-Jensen & Pedersen (2008) report typical length-to-width aspect ratios of 2.5. The reduced retention time can have important implications for plant fecundity, structural stability and habitat viability within canopies, as well as the transport and fate of pollutants and contaminants in both aquatic and terrestrial canopies.

As the canopy half-width, b, increases, there will be a width above which the vortices at the two flow-parallel edges no longer interact in a sympathetic manner. We anticipate that this transition occurs when the pressure perturbation at the canopy edges cannot translate across the canopy within half the time period of a passing vortex. Using the shallow water wave speed, $\sqrt{gh}$, to describe the translation speed of pressure perturbations, this threshold will occur at the point when $2b/\sqrt{gh} \gg 0.5T$, where T is the vortex period. In the cases shown in figure 14, $T = 10$ s and $2b/\sqrt{gh} = 0.2$ s, so it follows that vortices could communicate across the patch width. The vortex period was measured using the zero-crossings in the surface displacement record. The vortex period is largely set by the outer scale of the shear layer, δ_o, and thus by the water depth and friction coefficient (see White & Nepf 2003). For the same flow depth and bed conditions, and the maximum achievable flow speed of nearly 0.5 m s^{-1}, we would need a canopy of width 10–20 m in order to test the predicted disconnection of edge vortices. Unfortunately, this was not possibly within the flume available.

5. Conclusions

A set of experiments are presented for unidirectional flow through rectangular porous obstructions. Upstream of the canopy, the flow adjusts over a length scale proportional to the canopy width. The length scale of the interior adjustment region depends on the canopy flow-blockage, described by C_Dab. For high flow-blockage

canopies ($C_Dab \geqslant 2$), the adjustment length is set by the half-width, b. For low flow-blockage canopies ($C_Dab < 2$), the adjustment length is set by the canopy drag length scale, $(C_Da)^{-1}$.

Downstream of the adjustment region, shear layers form along the flow-parallel edges. Shear layer vortices form and grow to a finite size within this layer. The penetration of shear-layer vortices into the canopy scales with the drag length scale, i.e. $\delta_i = 0.5(C_Da)^{-1}$. The ratio of the vortex penetration length to the canopy half-width ($\delta_i/b = 0.5(C_Dab)^{-1}$) determines the dominant force driving the flow in the canopy interior. If $\delta_i < b$ ($C_Dab > 2$), the interior flow is governed by a balance between the pressure gradient and canopy drag. If $\delta_i \gtrsim b$ ($C_Dab < 2$), the interior flow is governed by a balance between the turbulent stress gradient and canopy drag. Thus, the flow-blockage parameter C_Dab, the ratio of the canopy width to the canopy drag length scale, controls both the behaviour of the flow adjustment regions as well as the behaviour in the canopy interior region.

When a porous obstruction has two interfaces parallel to the mean flow direction, the strength of the vortices that form on the flow-parallel edges is greatly increased relative to vortices that form at a single interface. With two interfaces, the vortices communicate across the canopy width and organize such that there is a phase shift of π radians with respect to each other. This organization enhances the vortex strength, measured by the Reynolds stress or v_{rms}, relative to identical canopies with a single flow parallel edge. The stronger vortices and the sympathetic response from both interfaces result in much higher turbulence within the canopy and, potentially, a significantly reduced residence time.

We thank the three anonymous reviewers who provided insightful comments that greatly improved this manuscript. This material is based upon work supported by a National Science Foundation (NSF) grant EAR 0738352. Any opinions, conclusions or recommendations expressed in this material are those of the author(s) and do not necessarily reflect the views of the NSF.

REFERENCES

Beavers, G. S. & Joseph, D. D. 1967 Boundary conditions at a naturally permeable wall. *J. Fluid Mech.* **30**, 197–207.

Belcher, S. E., Finnigan, J. J. & Harman, I. N. 2008 Flows through forest canopies in complex terrain. *Ecol. Appl.* **18** (6), 1436–1453.

Belcher, S. E., Jerram, N. & Hunt, J. C. R. 2003 Adjustment of a turbulent boundary layer to a canopy of roughness elements. *J. Fluid Mech.* **488**, 369–398.

Bentham, T. & Britter, R. 2003 Spatially averaged flow within obstacle arrays. *Atmos. Environ.* **37**, 2037–2043.

Bouma, T. J., van Duren, L. A., Temmerman, S., Claverie, T., Blanco-Garcia, A., Ysebaerty, T. & Herman, P. M. J. 2007 Spatial flow and sedimentation patterns within patches of epibenthic structures: combining field, flume and modelling experiments. *Cont. Shelf Res.* **27**, 1020–1045.

Brown, G. & Roshko, A. 1974 On density effects and large structure in turbulent mixing layers. *J. Fluid Mech.* **64**, 775–816.

Coceal, O. & Belcher, S. E. 2004 A canopy model of mean winds through urban areas. *Q. J. R. Met. Soc.* **130**, 1349–1372.

Drazin, P. & Reid, W. 1981 *Hydrodynamic Stability*. Cambridge University Press.

Eames, I., Hunt, J. C. R. & Belcher, S. E. 2004 Inviscid mean flow through and around groups of bodies. *J. Fluid Mech.* **515**, 371–389.

Finnigan, J. J. 2000 Turbulence in plant canopies. *Annu. Rev. Fluid Mech.* **32**, 519–571.

Finnigan, J. J. & Shaw, R. H. 2000 A wind-tunnel study of airflow in waving wheat: an EOF analysis of the structure of the large-eddy motion. *Boundary Layer Meteorol.* **96**, 211–255.

Gaylord, B., Rosman, J. H., Reed, D. C., Koseff, J. R., Fram, J., MacIntyre, S., Arkema, K., McDonald, C., Brzezinski, M. A., Largier, J. L., Monismith, S. G., Raimondi, P. T. & Mardian, S. 2007 Spatial patterns of flow and their modification within and around a giant kelp forest. *Limnol. Oceanogr.* **52** (5), 1838–1852.

Ghisalberti, M. & Nepf, H. M. 2002 Mixing layers and coherent structures in vegetated aquatic flows. *J. Geophys. Res.* **107** (C2), 3011.

Ghisalberti, M. & Nepf, H. M. 2009 Shallow flows over a permeable medium: the hydrodynamics of submerged aquatic canopies. *Transport in Porous Media* **78**, 309–326.

Gray, W. G. & Lee, P. C. Y. 1977 On the theorems for local volume averaging of multiphase systems. *Intl J. Multiphase Flow* **3** (4), 333–340.

Grimmond, C. S. B. & Oke, T. R. 1999 Aerodynamic properties of urban areas derived from analysis of surface form. *J. Appl. Meteorol.* **38** (9), 1262–1292.

Ho, C. & Huerre, P. 1984 Perturbed free shear layers. *Annu. Rev. Fluid Mech.* **16**, 365–424.

Jackson, G. A. 1997 Currents in the high drag environment of a coastal kelp stand off california. *Cont. Shelf Res.* **17** (15), 1913–1928.

Jackson, G. A. & Winant, C. D. 1983 Effect of a kelp forest on coastal currents. *Cont. Shelf Res.* **2** (1), 75–80.

Koch, D. L. & Ladd, A. J. C. 1997 Moderate Reynolds number flows through periodic and random arrays of aligned cylinders. *J. Fluid Mech.* **349**, 31–66.

Krzikalla, F. 2005 Numerical investigation of the interaction between wind and forest and heterogeneous conditions. Master's thesis, University of Karlsruhe.

Luhar, M., Coutu, S., Infantes, E., Fox, S. & Nepf, H. 2010 Wave-induced velocities inside a model seagrass bed. *J. Geophys. Res.* **115**, C12005.

Nepf, H. M., Ghisalberti, M., White, B. L. & Murphy, E. 2007 Retention time and dispersion associated with submerged aquatic canopies. *Water Resour. Res.* **43**, W04422.

Nikora, V., McEwan, I., McLean, S., Coleman, S., Pokrajac, D. & Walters, R. 2007 Double-averaging concept for rough-bed open-channel and overland flows: theoretical background. *J. Hydraul. Engng* **133** (8), 873–883.

Poggi, D., Katul, G. & Albertson, J. 2004*a* A note on the contribution of dispersive fluxes to momentum transfer within canopies. *Boundary Layer Meteorol.* **11** (3), 615–621.

Poggi, D., Porporato, A., Ridolfi, L., Albertson, J. D. & Katul, G. G. 2004*b* The effect of vegetation density on canopy sub-layer turbulence. *Boundary Layer Meteorol.* **111**, 565–587.

Raupach, M. R., Finnigan, J. J. & Brunet, Y. 1996 Coherent eddies and turbulence in vegetation canopies: the mixing layer analogy. *Boundary Layer Meteorol.* **78**, 351–382.

Raupach, M. R. & Shaw, R. H. 1982 Averaging procedures for flow within vegetation canopies. *Boundary Layer Meteorol.* **22**, 79–90.

Rosman, J. H., Koseff, J. R., Monismith, S. G. & Grover, J. 2007 A field investigation into the effects of a kelp forest (macrocystis pyrifera) on costal hydrodynamics and transport. *J. Geophys. Res.* **112**, C02016.

Sand-Jensen, K. & Pedersen, M. L. 2008 Streamlining of plant patches in streams. *Freshwat. Biol.* **53**, 714–726.

Schatz, M., Barkley, D. & Swinney, H. 1995 Instability in a spatially periodic open flow. *Phys. Fluids* **7** (2), 344–358.

Tamai, N., Asaeda, T. & Ikeda, H. 1986 Study on generation of periodical large surface eddies in a composite channel flow. *Water Resour. Res.* **22**, 1129–1138.

Tanino, Y. & Nepf, H. M. 2008 Laboratory investigation of mean drag in a random array of rigid, emergent cylinders. *J. Hydraul. Engng* **134** (1), 34–41.

Thom, A. S. 1971 Momentum absorption by vegetation. *Q. J. R. Meteorol. Soc.* **96**, 414–428.

Vogel, S. 1994 *Life in Moving Fluids: The Physical Biology of Flow*, 2nd edn. Princeton University Press.

White, B. L. & Nepf, H. M. 2007 Shear instability and coherent structures in shallow flow adjacent to a porous layer. *J. Fluid Mech.* **593**, 1–32.

Zong, L. & Nepf, H. 2010 Flow and deposition in and around a finite patch of vegetation. *Geomorphology* **116**, 363–372.